Int J Fract (2017) 205:169–188
DOI 10.1007/s10704-017-0189-z

ORIGINAL PAPER

# Fracture resistance testing of dissimilar nickel–chromium girth welds for clad line pipes

**Diego F. B. Sarzosa · Vitor S. Barbosa · Caio C. P. Santos · E. Hippert Jr. · C. Ruggieri**

Received: 22 July 2016 / Accepted: 27 January 2017 / Published online: 22 February 2017


**Abstract** This work presents an experimental investigation of the ductile tearing properties for the girth weld of a typical C–Mn pipe internally clad with ASTM UNS N06625 Alloy 625 using measured crack growth resistance curves ($J-\Delta a$ and CTOD$-\Delta a$ curves). Here, the material of the external pipe is a typical API 5L Grade X65 pipeline steel whereas the inner clad layer is made of a nickel–chromium corrosion resistant alloy steel. Testing of the girth weld employed side-grooved, clamped SE(T) specimens with a weld centerline notch to determine the crack growth resistance curves based upon the unloading compliance method using a single specimen technique. This experimental characterization provides additional toughness data which serve to evaluate the effectiveness of current procedures in determining accurate experimentally measured $R$-curves for this class of material, including the effects of weld strength mismatch.

D. F. B. Sarzosa · Vitor S. Barbosa · C. Ruggieri (✉)
Department of Naval Architecture and Ocean Engineering, University of São Paulo, São Paulo, Brazil
e-mail: claudio.ruggieri@usp.br

C. C. P. Santos
Department of Mechanical Engineering, University of São Paulo, São Paulo, Brazil

E. Hippert Jr.
Petrobras Development and Research Center (TMEC-CENPES), Rio de Janeiro, Brazil

**Keywords** Fracture resistance test · $J$-integral · CTOD · Unloading compliance method · SE(T) specimen · Girth weld · Clad line pipe

## 1 Introduction

The increasing demand for energy and natural resources has spurred a flurry of exploration and production of oil and natural gas in more hostile environments, including very deep water offshore hydrocarbon reservoirs. One of the key challenges facing the oil and gas industry is the assurance of more reliable and fail-safe operations of the infrastructure for production and transportation. Currently, structural integrity of submarine risers and flowlines conducting corrosive and aggressive hydrocarbons represents a key factor in operational safety of subsea pipelines. Advances in existing technologies favor the use of C–Mn steel pipelines either clad or mechanically lined with corrosion resistant alloys (CRA), such as ASTM UNS N06625 Alloy 625 (American Society for Testing and Materials 2009, 2011a), for the transport of corrosive fluids. Accurate measurements of fracture resistance properties, including crack growth resistance curves of the girth weld material, become essential in defect assessment procedures of the weldment region and the heat affected zone, where undetected crack-like defects (such as lack of penetration, deep undercuts, root cracks, etc.) may further extend due to to the high tension stresses and strains. However, while cost effective, fracture assessments of

girth welds in lined pipes become more complex due to the dissimilar nature of these materials.

Fracture mechanics based approaches to describe ductile fracture behavior in structural components, including welded structures, rely strongly on crack growth resistance ($J-\Delta a$ or, equivalently, CTOD$-\Delta a$) curves (also termed $R$-curves), to describe crack extension followed by crack instability of the material (Hutchinson 1983; Anderson 2005); here, either the $J$-integral or the crack-tip opening displacement (CTOD or $\delta$) describe the intensity of near-tip deformation (Hutchinson 1983; Anderson 2005) and $\Delta a$ is the amount of crack growth. These approaches allow the specification of critical crack sizes based on the predicted growth of crack-like defects under service conditions. Current defect assessment methodologies applicable to marine risers and submarine pipelines (see, e.g., DNV OS-F101 Det Norske Veritas 2013) advocate the use of single edge notch tension specimens (often termed SE(T) or SENT crack configurations) to measure experimental $R$-curves to characterize the increase in toughness of pipeline girth welds during ductile crack growth. The primary motivation to use SE(T) fracture specimens in defect assessment procedures for this category of structural components is the strong similarity in crack-tip stress and strain fields which drive the fracture process for both crack configurations (Nyhus et al. 2003; Cravero and Ruggieri 2005; Silva et al. 2006; Shen et al. 2008). However, while now utilized effectively in fracture testing of pipeline girth welds with limited overmatch, strong mismatch between the weld metal and base plate strength potentially affects the macroscopic mechanical behavior of the specimen in terms of its load–displacement response with a potentially strong impact on the crack growth resistance curve. Moreover, with the increased use of higher strength pipeline steels, unintended weld strength undermatching emerges as a likely possibility which thus raises strong concerns in integrity assessments of field girth welds produced in lined pipes having circumferential flaws.

Much recent research has focused on the development of standardized procedures for crack growth resistance testing using SE(T) fracture specimens. Essentially all these efforts adopt primarily the unloading compliance method based upon testing of a single specimen. Implementation of the method essentially follows conventional procedures to determine the instantaneous value of the specimen compliance at partial unloading during the measurement of the load versus displacement curve thereby enabling accurate estimations of $J$ (or $\delta$) and $\Delta a$ at several locations on the load–displacement records from which the $J-R$ and $\delta-R$ curves can be developed. While the methodology simply broadens the current framework for fracture testing of three-point bend and compact tension specimens, such as ASTM E1820 (American Society for Testing and Materials 2011b), there is not much consensus on specific requirements to obtain $J$-integral and CTOD parameters, as well as the amount of crack extension, including the estimation procedure for toughness values and compliance equations. Since the evaluation of all fracture toughness quantities represents a key step in accurate laboratory measurements of fracture resistance curves, differences in $J$ and CTOD estimation equations or different compliance equations affect the experimentally measured crack growth resistance behavior thereby complicating the definition of meaningful toughness data. This picture is further complicated by the potential effect of the clad layer (which is an integral part of the SE(T) specimen extracted from girth weld clad pipes) on the mechanical response of the fracture specimen thereby affecting the amount of crack extension with increased macroscopic loading, as characterized by $J$ or CTOD.

This work presents an exploratory investigation of the ductile tearing properties for the girth weld of a typical C–Mn pipe internally clad with a nickel–chromium corrosion resistant alloy (CRA) using experimentally measured crack growth resistance curves ($J-\Delta a$ curves). Here, the material of the external pipe is a typical API 5L Grade X65 pipeline steel with a high yield stress of 620 MPa and relatively low hardening properties whereas the inner clad layer is made of ASTM UNS N06625 Alloy 625 with yield stress of 462 MPa and high hardening. The high mechanical strength and superior resistance to a wide range of corrosive environments of unusual severity for this material derive from the combination of the nickel–chromium matrix with other microalloying elements such as molybdenum and niobium. Testing of the pipeline girth weld employed side-grooved, clamped SE(T) specimens with a weld centerline notch to determine the crack growth resistance curves based upon the unloading compliance (UC) method using a single specimen technique and load–displacement records. The resistance curves are first determined on the basis of the procedure developed by Cravero and Ruggieri (2007a) and

Mathias et al. (2013) to evaluate crack growth resistance data using estimation equations for $J$ and $\Delta a$ based on plane-strain conditions. The analyses then consider evaluation of $J$-resistance data from newly developed results to estimate $J$ and $\Delta a$ from 3-D finite element computations of weld centerline notched SE(T) specimens incorporating the clad layer and the experimental stress–strain response of the weldment. Finally, we compare the crack growth resistance curves defined in terms of $\delta - \Delta a$ data for which the CTOD is determined on the basis of $J$–CTOD relationships and the double clip gage (DCG) technique. These results are further compared with crack growth resistance data derived from a digital image correlation (DIC) method to measure the CTOD directly from the deformed crack flank for the extending crack. This exploratory experimental characterization provides additional toughness data which serve to evaluate the effectiveness of current procedures in determining experimentally measured $R$-curves for this class of material.

## 2 Fracture resistance test procedure

Conventional testing programs to measure crack growth resistance curves in ductile materials routinely employ an unloading compliance (hereafter denoted UC) technique using a single specimen. Implementation of the method essentially follows from determining the instantaneous value of the specimen compliance at partial unloading during the measurement of load versus displacement data in which the experimental value of $J$ derives from the plastic contribution to the strain energy for the cracked specimen (Anderson 2005; Kanninen and Popelar 1985; Ruggieri 2012). This section briefly describes the analytical relationships to determine fracture resistance curves for SE(T) specimens using the unloading compliance technique and the $\eta$-method. Only salient features of the estimation procedure for $J$ (or CTOD) and $\Delta a$ are discussed here. Readers are referred to the works of Joyce et al. (1993), Cravero and Ruggieri (2007a, b), Ruggieri (2012), Mathias et al. (2013) and Zhu and McGaughy (2014) for details.

### 2.1 Experimental evaluation of the $J$-integral

A widely used approach (which forms the basis of current standards such as ASTM E1820 American Society for Testing and Materials 2011b) to evaluate $J$ with crack extension follows from an incremental procedure which updates $J_e$ and $J_p$ at each partial unloading point, denoted $k$, during the measurement of the load versus displacement curve and described in the form

$$J^k = J_e^k + J_p^k \tag{1}$$

where the current elastic term is simply given by

$$J_e^k = \left(\frac{K_I^2}{E'}\right)_k \quad . \tag{2}$$

Here, $K_I$ is the elastic stress intensity factor for the cracked configuration with plane-strain conditions adopted such that $E' = E/(1-\nu^2)$ where $E$ and $\nu$ are the (longitudinal) elastic modulus and Poisson's ratio, respectively

The plastic term, $J_p^k$, can be evaluated by an incremental formulation in terms of crack mouth opening displacement (CMOD) proposed by Cravero and Ruggieri (2007b) and Zhu et al. (2008) in the form

$$J_p^k = \left[J_p^{k-1} + \frac{\eta_{J-CMOD}^{k-1}}{b_{k-1} B_N}\left(A_p^k - A_p^{k-1}\right)\right] \cdot \Gamma_k \tag{3}$$

with $\Gamma_k$ defined by

$$\Gamma_k = \left[1 - \frac{\gamma_{LLD}^{k-1}}{b_{k-1}}\left(a_k - a_{k-1}\right)\right] \tag{4}$$

where factor $\gamma_{LLD}$ is evaluated from

$$\gamma_{LLD} = \left[-1 + \eta_{J-LLD}^{k-1} - \left(\frac{b_{k-1}}{W \eta_{J-LLD}^{k-1}} \frac{d\eta_{J-LLD}^{k-1}}{d(a/W)}\right)\right]. \tag{5}$$

In the above, $A_p$ is the plastic area under the load–displacement curve, $B_N$ is the net specimen thickness at the side groove roots, $b$ is the uncracked ligament ($b = W - a$ where $W$ is the width of the specimen and $a$ is the crack length) and factor $\eta$ represents a nondimensional parameter which relates the plastic contribution to the strain energy for the cracked body and $J$. See Cravero and Ruggieri (2007b) and Mathias et al. (2013) for further details.

The incremental expressions for $J_p$ defined by Eqs. (3)–(5) contain two contributions: one is from the plastic work in terms of CMOD and, hence, $\eta_{J-CMOD}$

and the other is due to crack growth correction in terms of LLD by means of $\eta_{J-LLD}$. While the resulting $J$-estimation procedure based on CMOD may appear a little more complex, evaluation of the above expressions is also relatively straightforward provided the two geometric factors, $\eta_{J-CMOD}$ and $\eta_{J-LLD}$, are known. Here, we follow Mathias et al. (2013) and adopt plane-strain expressions for the $\eta$-factors applicable to clamped SE(T) specimens with clamped distance, $H$, over specimen with ratio, $H/W = 10$, as

$$\eta_{J-CMOD} = 1.067 - 1.767\frac{a}{W} + 7.808\left(\frac{a}{W}\right)^2 - 18.269\left(\frac{a}{W}\right)^3 + 15.295\left(\frac{a}{W}\right)^4 - 3.083\left(\frac{a}{W}\right)^5 \tag{6}$$

$$\eta_{J-LLD} = -0.623 + 9.336\frac{a}{W} - 4.584\left(\frac{a}{W}\right)^2 - 47.963\left(\frac{a}{W}\right)^3 + 87.697\left(\frac{a}{W}\right)^4 - 44.875\left(\frac{a}{W}\right)^5 \tag{7}$$

## 2.2 Estimation of crack extension

The estimation of crack length based on the unloading compliance (UC) technique is a key step in the testing protocol to measure the crack growth resistance response using a single-specimen test. The slope of the load–displacement curve during the $k$th unloading defines the current specimen compliance, denoted $C_k$ ($C = V/P$, where $V$ is the CMOD and $P$ represents the applied load), which depends on specimen geometry and crack length. For SE(T) crack configurations, the normalized specimen compliance based on CMOD is defined as

$$\mu = \left[1 + \sqrt{E' B_e C_{CMOD}}\right]^{-1} \tag{8}$$

and $B_e$ is the effective thickness defined by

$$B_e = B - \frac{(B - B_N)^2}{B} \quad . \tag{9}$$

In the above expression defining the normalized compliance, $E' = E/(1-\nu^2)$ or $E' = E$ whether plane-strain or plane-stress conditions are assumed. In the remaining of this article, we follow Cravero and Ruggieri (2007a) and adopt plane-strain conditions to define $\mu$ in previous Eq. (8)—note that ASTM E1820 (American Society for Testing and Materials 2015) adopts plane-stress rather than plane-strain to define $\mu$ for conventional fracture specimens.

The current crack length follows directly from measuring the instantaneous compliance during unloading of the specimen once the functional dependence of crack length and specimen compliance is available. For the clamped SE(T) specimen with $H/W = 10$ analyzed here, Cravero and Ruggieri (2007a) provide the relationship between $a/W$ and $\mu$ as

$$a/W = 1.6485 - 9.1005\mu + 33.025\mu^2 - 78.467\mu^3 + 97.344\mu^4 - 47.227\mu^5 \tag{10}$$

which is valid in the range $0.1 \le a/W \le 0.7$.

## 2.3 CTOD evaluation procedure

The previous framework also applies when the CTOD is adopted to characterize the crack-tip driving force. To the extent that $J$ describes the crack-tip conditions with increased crack extension and, further, that a unique $J-$CTOD relationship holds true for stationary and growing cracks, both $J-\Delta a$ and CTOD$-\Delta a$ curves equally characterize well the crack growth resistance behavior for the tested material (Hutchinson 1983; Anderson 2005). Here, we follow the work of Sarzosa et al. (2015) and adopt an evaluation procedure for the crack tip opening displacement (CTOD) derived directly from experimentally measured records of load versus crack mouth opening displacement (CMOD). The methodology essentially determines the CTOD value from first evaluating the plastic component of $J$ using the plastic work defined by the area under the load versus CMOD curve and then converting it into the corresponding value of plastic CTOD. The approach has the potential to simplify evaluation of CTOD values while, at the same time, relying on a rigorous energy release rate definition of $J$ for a cracked body yielding the expression (Anderson 2005; Sarzosa et al. 2015; Kirk and Dodds 1993; Kirk and Wang 1995; Zhu and Joyce 2012)

$$\delta = \frac{J}{m\sigma_0} \tag{11}$$

in which $m$ represents a proportionality coefficient strongly dependent on the material strain hardening but weakly sensitive to crack size as characterized by the

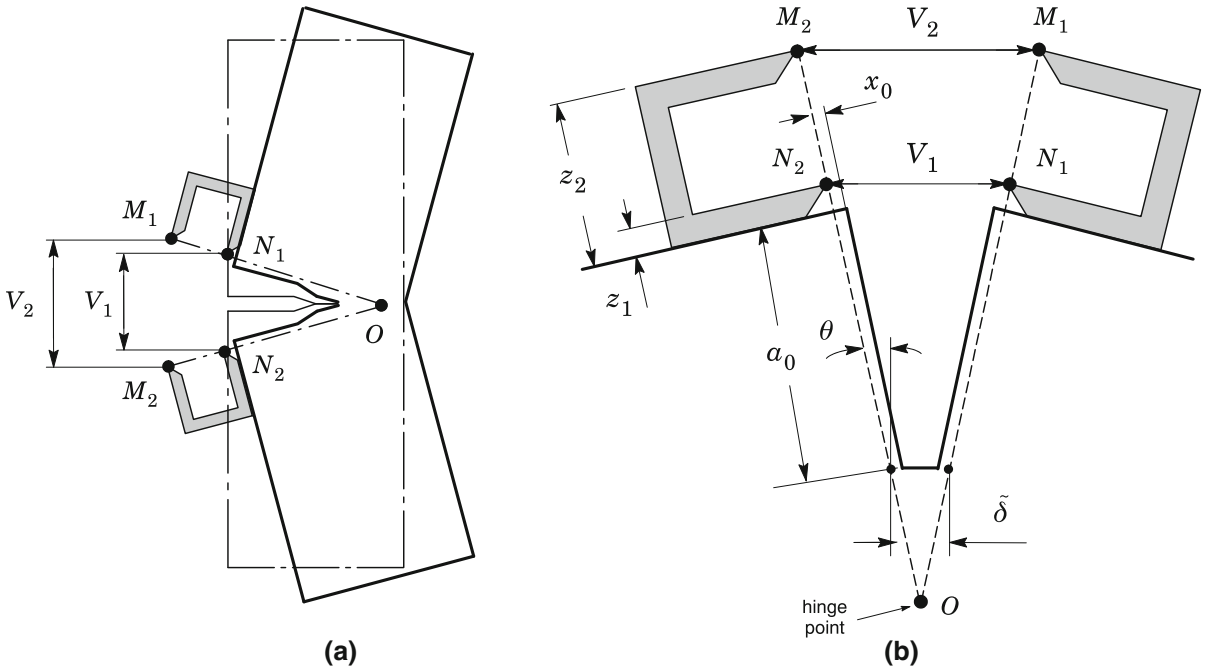


**Fig. 1** Double clip-gage method to estimate the CTOD using measurements of crack opening displacements (COD) at two different points

$a/W$-ratio. In the above, $\sigma_0$ defines a reference stress value, usually taken as the material yield stress, $\sigma_{ys}$, or the flow stress, $\sigma_f$, defined by $\sigma_f = (\sigma_{uts} + \sigma_{ys})/2$ in which $\sigma_{uts}$ denotes the tensile strength. The choice of $\sigma_0$ has little effect on the absolute value of the CTOD provided a consistent $m$-value is used in the evaluation procedure. A number of studies utilize $\sigma_{ys}$ (Shih 1981; Kudari and Kodancha 2008; Huang and Zhou 2014) whereas other works (Kirk and Dodds 1993; Kirk and Wang 1995), including ASTM E1820 (American Society for Testing and Materials 2011b), adopt $\sigma_f$ to make the results less sensitive to the actual strain hardening behavior of the material.

For plane-strain conditions and using a simple power-hardening model to characterize the uniaxial true stress ($\bar{\sigma}$) versus logarithmic strain ($\bar{\epsilon}$) in the form

$$\frac{\bar{\epsilon}}{\epsilon_{ys}} = \frac{\bar{\sigma}}{\sigma_{ys}}, \epsilon \le \epsilon_{ys} \; ; \quad \frac{\bar{\epsilon}}{\epsilon_{ys}} = \left(\frac{\bar{\sigma}}{\sigma_{ys}}\right)^n, \epsilon > \epsilon_{ys} \quad (12)$$

where $\sigma_{ys}$ and $\epsilon_{ys}$ are the yield stress and strain, and $n$ is the strain hardening exponent, Sarzosa and Ruggieri (2014) arrived at a functional dependence of parameter $m$ with crack size, $a/W$, and hardening exponent, $n$, in the form

$$m = 1.147 - 0.420(a/W) + 0.672(a/W)^2 + 2.859n^{-1} - 0.002n \quad (13)$$

which is valid in the range $0.2 \le a/W \le 0.7$, $5 \le n \le 20$. Here, we note that the above expression derives from taking $\sigma_f$ as $\sigma_0$ in previous Eq. (11) and rearranging the formula given in Sarzosa and Ruggieri (2014).

To provide a simpler extension of the plastic hinge concept applicable to broader crack configurations, a double clip-gage arrangement can also be used as an alternative method to estimate the CTOD from adequate measurements of crack opening displacements (COD) at two different points. Figure 1a, b schematically illustrates the essential features of the procedure in which a pair of knife edges is attached on each side of the notch close to the notch mouth to allow the use of two clip-gages to measure the displacement at these knife edge positions—such double clip-gage (DCG) fixture is currently recommended by recent test procedures to evaluate resistance curves using SE(T) specimens (Upstream ExxonMobil 2010; British Institution 2014; Pussegoda et al. 2014). With the method illustrated in Fig. 1, a simple geometrical approach then enables defining the CTOD ($\delta$) in terms of the two mea-

sured COD-values. Here, the double clip-gage arrangement shown in Fig. 1 deserves attention since the DCG mounting fixture is typically installed at a distance $x_0$ from the notch flank as shown in Fig. 1b; only when $x_0 = 0$ can the DCG fixture be considered aligned with the specimen machined notch and the fatigue precrack. This practice results in an *apparent* offset of the crack flank thereby potentially increasing the measured CTOD, here denoted as $\tilde{\delta}$ in the figure. The specification of $x_0$ in the test protocol introduces an explicit dimension in the test procedure and opens the possibility to correct the measured CTOD$-R$ curve for different values of $x_0$. However, this option was not examined in the present study so that hereafter we refer to $\tilde{\delta}$ as $\delta$ for simplicity while, at the same time, enabling direct comparisons with CTOD$-R$ curves derived from current procedures (Upstream ExxonMobil 2010; British Institution 2014; Pussegoda et al. 2014).

Now, by measuring two COD-values, $V_1$ and $V_2$, at two locations on a straight line passing through the crack flank of the specimen and assuming rigid body rotation, the specimen rotation angle yields

$$\sin\theta = \frac{V_1 - \delta}{2(z_1 + a_0)} = \frac{V_2 - V_1}{2(z_2 - z_1)} \tag{14}$$

from which a geometrical relationship between the CTOD ($\delta$) and both measured COD-values is obtained in the form

$$\delta = V_1 - \frac{z_1 + a_0}{z_2 - z_1}(V_2 - V_1) \tag{15}$$

where $z_1$ and $z_2$ represent the distance of the measuring points for $V_1$ and $V_2$ from the specimen surface as depicted in Fig. 1b. Here, we note that the crack size, $a_0$, entering into Eq. (15) represents the initial crack length not the current crack size measured at the extending tip as discussed by Sarzosa et al. (2015). Moreover, also observe that the CTOD is defined here as the crack opening at the position of the original crack tip such that, with crack-tip blunting, the position of the original crack tip falls slightly behind the current crack tip.

### 2.4 Rotation correction

The specimen compliance, $C$, needed to determine the crack length may not reflect changes in specimen geometry due to specimen rotation as the test progresses. Specimen rotation shifts the measurement points for the applied load and CMOD with reference to the original (undeformed) configuration upon which the specimen compliance, $C$, is based on. Here, we adopt the following expression to correct the specimen compliance developed by Shen and Tyson (2009) given by

$$\tilde{C}_k = \frac{C_k}{1 - [0.165(a_0/W)(P_k/P_Y)]} \tag{16}$$

where $\tilde{C}_k$ is the specimen compliance at the $k$th unloading corrected for specimen rotation, $a_0$ is the original crack size, $W$ denotes the specimen width and $P_Y = \sigma_f B_N(W - a)$ defines the limit load of the clamped SE(T) specimen with $\sigma_f$ representing the flow stress as already defined above.

## 3 Experimental details

### 3.1 Material description and welding procedure

The material utilized in this study was a girth weld of a typical API 5L Grade X65 pipe internally clad with a nickel–chromium corrosion resistant alloy (CRA) made of ASTM UNS N06625 Alloy 625 (American Society for Testing and Materials 2009, 2011a). The tested weld joint was made from an 8-inch pipe (203 mm outer diameter) having overall thickness, $t_w = 19$ mm, which includes a clad layer thickness, $t_c = 3$ mm. Girth welding of the pipe was performed using 100%$CO_2$ gas-shielded FCAW process in the 5G (horizontal) position with a single V-groove configuration in which the root pass was made by TIG welding in the 2G (vertical) position. The main weld parameters used for preparation of the test weld using the FCAW process are: (1) welding current 200−250 A; (2) welding voltage 27−29 V; (3) average wire feed speed of 11−12 m/min. A nickel–chromium filler metal matching the ASTM UNS N06625 Alloy 625 (American Society for Testing and Materials 2009, 2011a), was employed to produce the girth weld so that the clad internal layer and the weld metal have very similar mechanical properties. Since the girth weld was specifically produced to extract weld centerline notched SE(T) specimens for evaluation of crack growth resistance properties in nickel–chromium girth welds made in clad line pipes, no layers of buttering material were applied at the inside surface and root pass of the weld joint.

**Table 1** Tensile properties of tested girth weld at room temperature (20 °C) measured from subsize specimens with 6 mm as per ASTM E8M (American Society for Testing and Materials 2011c)

| Material | $\sigma_{ys}$ (MPa) | $\sigma_{uts}$ (MPa) | $E$ (MPa) | $\sigma_{ys}/\sigma_{uts}$ | $n$ |
|---|---|---|---|---|---|
| Base plate | 620 | 700 | 200,150 | 0.89 | 18.9 |
| Weld metal | 462 | 627 | 157,500 | 0.74 | 9.7 |

$\sigma_{ys}$ and $\sigma_{uts}$ denote the yield stress and tensile strength

Table 1 provides the mechanical properties of the base plate material and the weld metal at room temperature (20 °C) in which the measured values are based on standard tensile testing using subsize specimens with 6 mm diameter. The material of the external pipe has a high yield stress of 620 MPa and relatively low hardening properties whereas the inner clad layer has yield stress of 462 MPa and high hardening. Here, we note that the measured yield stress for the external pipe is slightly higher than the maximum value of 600 MPa specified by API 5L PSL-2 (American Petroleum Institute 2007b) for grade X65 steel - observe, however, that the yield stress to tensile strength ratio is $\sigma_{ys}/\sigma_{uts} = 0.89$, which is below the maximum specified value of 0.93 for this steel. Based on Annex F of API 579 (American Petroleum Institute 2007a), the Ramberg–Osgood strain hardening exponents describing the stress–strain response for the base plate and weld metal are estimated as $n_{BM} = 18.9$ and $n_{WM} = 9.7$. The measured tensile properties indicate that the weldment undermatches the base plate material by ≈25% at room temperature—also observe a relatively strong mismatch in hardening behavior as characterized by the large differences in the hardening exponents. Moreover, because of the mismatch in strain hardening behavior, it can be easily anticipated that, after some amount of plastic deformation in the range of ≈2%, the weld metal overmatches the base plate material.

The elastic properties for the tested materials displayed in Table 1 also deserves attention. Specifically, we note the relatively low elastic modulus defined by $E \approx 158$ GPa for the weld metal compared to $E \approx 200$ GPa corresponding to the API 5L Grade X65 pipe material. While still comparable, the weld metal value is undoubtedly lower than might be expected for typical elastic properties of an ASTM UNS N06625 Alloy 625. Since the tensile properties, including the elastic modulus, given in Table 1 actually refer to the nickel–chromium filler metal matching the ASTM UNS N06625 Alloy 625 to produce the girth weld, we argue that dilution of two different materials (i.e., ASTM UNS N06625 Alloy 625 and API 5L Grade X65) may have caused a certain amount of degradation in the properties of the weldment—as noted before, no layers of buttering material were used to produce the girth weld. Unfortunately, the precise source of this behavior remains unclear at present. However, this measured value of the elastic modulus for the weld metal fits adequately into the present crack growth analysis since the predicted and measured amounts of ductile tearing for the tested specimens fall within a very acceptable margin as described later.

### 3.2 Specimen geometry

Unloading compliance (UC) tests at room temperature were performed on weld centerline notched SE(T) specimens with fixed-grip loading extracted from the girth weld of the pipe specimen in the longitudinal direction as illustrated in Fig. 2a to measure tearing resistance curves in terms of $J-\Delta a$ and CTOD–$\Delta a$. The tested SE(T) specimens have $a/W = 0.3$ and $H/W = 10$ with thickness $B = 16$ mm, width $W = 16$ mm and clamp distance $H = 160$ mm as illustrated in Fig. 2b. Here, $a$ is the crack depth and $W$ is the specimen width which is slightly smaller than the pipe thickness, $t_w$. Conducted as part of a collaborative program between the University of São Paulo and Petrobras, testing of these specimens focused on the evaluation of crack growth resistance data for nickel–chromium girth welds made in clad line pipes.

The specimens were pre-cracked in bending using a three-point bend apparatus very similar to a conventional three-point bend test. After fatigue pre-cracking, the specimens were side-grooved to a net thickness of ∼85% the overall thickness (7.5% side-groove on each side) to promote uniform crack growth and tested following some general guidelines described in Rug-

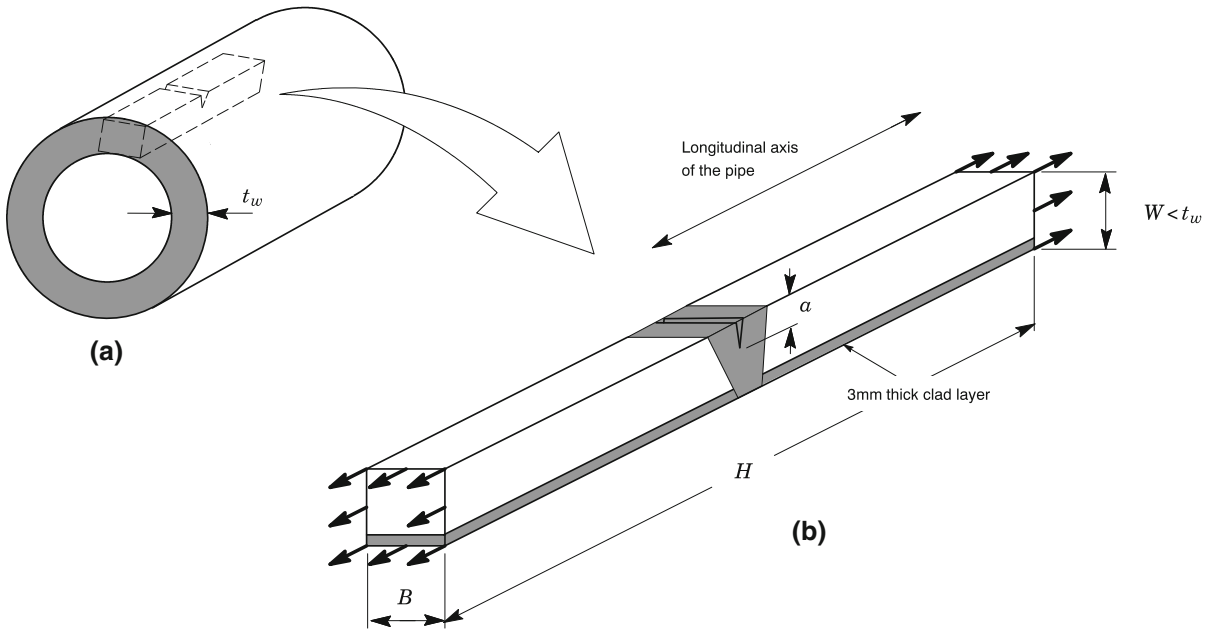


**Fig. 2** Geometry of tested weld centerline notched SE(T) specimens with fixed-grip loading extracted from the girth weld of the pipe specimen in the longitudinal direction

gieri and Hippert (2015). Records of load versus crack mouth opening displacements (CMOD) were obtained for the specimens using a clip gage mounted on knife edges attached to the specimen surface. The test program covered four specimens, one of them instrumented with a double clip gage fixture as required for CMOD measurements at two different points [refer to Fig. (1) and Ruggieri and Hippert (2015)] for evaluation of the CTOD using the DCG method as described later in Sect. 5.5.

## 4 Numerical analysis of 3-D models for weld centerline notched specimens

The resistance curves reported in the present investigation derive from plane-strain results for $\eta$-factors and compliance solutions obtained by Mathias et al. (2013) and Cravero and Ruggieri (2007a). These results are cast in terms of Eqs. (6), (7) and (10), which are essentially applicable to homogeneous materials. Recent test procedures to evaluate resistance curves using SE(T) specimens (Upstream ExxonMobil 2010; British Institution 2014; Pussegoda et al. 2014) also adopt 2-D formulations to describe the key quantities entering into the fracture resistance evaluation method. Because the tested fracture specimens incorporate a clad layer having a relatively strong mismatch in flow properties (refer to Fig. 8; Table 1) within the bulk of the specimen, application of the framework outlined previously may be questioned as it may not accurately describe the specimen response in terms of the evolution of load with CMOD. This section provides details of the numerical analyses for the weld centerline notched SE(T) specimens having a clad layer.

Nonlinear finite element analyses are described for 3-D models of SE(T) fracture specimens with fixed clamp distance over specimen width ratio, $H/W = 10$, and cross section dimensions defined by specimen width, $W = B = 16$ mm. The analysis matrix includes 15% side-grooved crack configurations (7.5% side-groove on each side) having varying crack sizes in the range $a/W = 0.1$–$0.7$ with increments of 0.1 The weld bevel geometry is represented by a V-shaped groove with an included angle of 50° and a root gap of 3 mm—these values characterize well the actual weldment obtained to produce the test specimens. The weld fracture specimen is modeled as a bimaterial component with no transition region such that the mechanical properties for the heat affected zone (HAZ) are not considered. Moreover, a uniform clad layer of thickness, $t_c = 3$ mm, is placed at the bottom of the specimen as shown in Fig. 2b. As already mentioned in Sect. 3.1, the clad

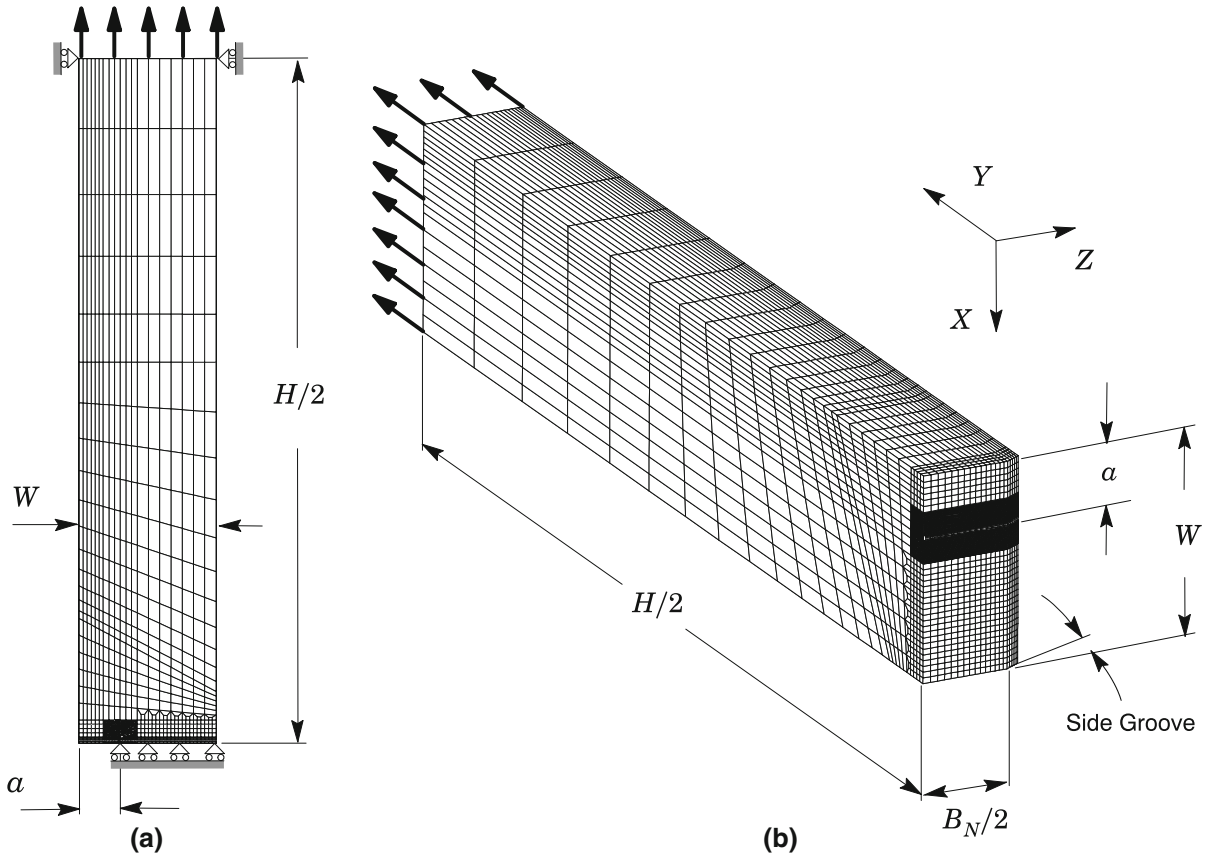


**Fig. 3** Typical finite element model for the weld centerline notched SE(T) specimens having a clad layer with $a/W = 0.3$: **a** In-plane mesh and detail of the blunt notch model; **b** Quarter-symmetric 3-D finite element model

internal layer and the weld metal are considered to have the same mechanical properties as described in Table 1.

Figure 3 shows the finite element model constructed for the 3-D analyses of the clamped SE(T) specimen having $a/W = 0.3$. All other crack models have very similar features. A conventional mesh configuration having a focused ring of elements surrounding the crack front is used with a small key-hole at the crack tip; the radius of the key-hole, $\rho_0$, is 3 μm (0.003 mm) to enhance computation of $J$-values at low deformation levels. Previous numerical analyses (Cravero and Ruggieri 2005) reveal that such mesh design provides detailed resolution of the near-tip stress–strain fields which is needed for accurate numerical evaluation of $J$-values. Symmetry conditions permit modeling of only one-quarter of the specimen with appropriate constraints imposed on the symmetry planes. A typical quarter-symmetric, 3-D model has 20 variable thickness layers with ∼42, 000 8-node, 3D elements (∼48, 000 nodes) defined over the half-thickness $(B/2)$; the thickest layer is defined at $Z = 0$ with thinner layers defined near the side groove root region $(Z = 0.425B)$ to accommodate strong $Z$ variations in the stress distribution. Here, the side-grooves are introduced in the numerical model as follows: (1) the $Y$-constraints on crack-plane nodes for which $X = 0$ and $Z > 0.425B$ (these nodes correspond to the 4 outermost layers) are first released; (2) these nodes are translated in the $Y$ direction according to a linear mapping corresponding to a side-groove half-angle of 30°. Since the primary interest here lies in the effect of side-grooves on the load–displacement response, the notch radius of the side-groove is not modeled. These numerical models are loaded by displacement increments acting in the $Y$-direction imposed on the loading points to enhance numerical convergence with increased levels of deformation. Moreover, the rigid grip conditions associated with the clamped ends of the specimen are modeled by imposing $X$-direction constraints (in case of 2-D plane-strain models), and $X$-direction and $Z$-

direction (in case of 3-D models) on nodes defined at $Z = H/2$ (see Fig. 3).

The evolution of load with increased displacement required for computations of specific solutions for the $\eta$-factor and compliance function is generated by the finite element code WARP3D (Healy et al. 2014). To construct the relationship between $a/W$ and specimen compliance, $\mu$, a series of linear elastic analyses provides the load–displacement ratios for all fracture models. These analyses adopt the elastic constants values for the base plate and weld metal given in Table 1 with $\nu = 0.3$. Evaluation of the geometric factors, $\eta_{J-CMOD}$ and $\eta_{J-LLD}$, follows from performing numerical analyses on the fracture models using an elastic-plastic constitutive law incorporating a flow theory with conventional Mises plasticity in small geometry change (SGC) setting. The mechanical and flow properties for the weldment and clad layer described previously were utilized to generate the required numerical solutions reported here.

## 5 Results and discussion

### 5.1 Compliance and $\eta$-factor solutions for the clad SE(T) specimen

Before launching into the evaluation of crack growth resistance curves addressed next, we first provide the compliance and $\eta$-factor solutions for the tested weld centerline notched SE(T) specimens having a clad layer obtained from the 3-D analyses described previously. These 3-D results have a direct bearing on the fracture resistance data if a connection is made between improved values of $J$ (CTOD) and $\Delta a$ with new solutions for $\eta$, $\mu$ and parameter $m$.

Here, evaluation of the geometric factors, $\eta_{J-CMOD}$ and $\eta_{J-LLD}$, as well as the relationship between $a/W$ and $\mu$ is performed following the procedures described in Cravero and Ruggieri (2007a) and Ruggieri (2012). By using the evolution of load with increased displacement for the numerical models of the clad SE(T) specimens, we arrive at more specific solutions for $\eta$-factors given as

$$\eta_{J-CMOD} = 1.437 - 3.112\frac{a}{W} + 15.628\left(\frac{a}{W}\right)^2 - 45.767\left(\frac{a}{W}\right)^3 + 58.667\left(\frac{a}{W}\right)^4 - 27.667\left(\frac{a}{W}\right)^5 \quad (17)$$

$$\eta_{J-LLD} = -0.684 + 15.626\frac{a}{W} - 35.142\left(\frac{a}{W}\right)^2 + 2.625\left(\frac{a}{W}\right)^3 + 69.208\left(\frac{a}{W}\right)^4 - 59.001\left(\frac{a}{W}\right)^5 \quad (18)$$

whereas an improved relationship between crack length and normalized compliance, as defined previously by Eq. (8) in terms of plane-strain conditions, is given by

$$a/W = 1.9215 - 13.2195\mu + 58.7080\mu^2 - 155.2823\mu^3 + 207.3987\mu^4 - 107.9176\mu^5 \quad (19)$$

which are valid in the range $0.1 \le a/W \le 0.7$. As shown in the next sections, the resulting fracture resistance curves on the basis of the above formulations are in slightly better agreement with DIC measurements since they account for 3-D effects as well as reflecting the mismatch behavior in flow properties between the weld metal, including the clad layer, and the base plate material not captured in the plane-strain formulation described by Eqs. (6), (7) and (10).

An improved $J-$CTOD relationship is also of interest. Evaluation of parameter $m$ entering into Eq. (11) follows from the evolution of $J$ with CTOD for the 3-D numerical models of the weld centerline notched specimens described in Sect. 4 leading to

$$m = 1.932 - 1.845(a/W) + 1.654(a/W)^2 \quad (20)$$

which is also valid in the range $0.1 \le a/W \le 0.7$.

Figure 4a–d compares the above expressions needed to evaluate the fracture resistance curves in terms of $J$ and CTOD with the plane strain solutions provided in Sect. 2, which derive from numerical analyses for a homogeneous material. In these plots, the solid lines represent the plane-strain results in which the variation of $\eta_{J-CMOD}$, $\eta_{J-LLD}$ and $m$ with $a/W$ is determined by using Eqs. (6), (7) and (13) in conjunction with a strain hardening exponent of 9.7 (which corresponds to the $n$-value for the weld metal), whereas the dashed lines describe the 3-D results for the weld centerline notched SE(T) specimen having a clad layer. The significant features include: (1) the 3-D $\eta$-factors for the weld centerline notched SE(T) specimen having a clad layer are higher than the corresponding plane-strain values for a homogeneous material; here, differences range from ≈30% for the shallow crack specimen to ≈20−25% for the deeply cracked specimen; (2) apart from the shallow crack range ($0.1 \le a/W \le 0.2-0.3$), the $J-$CTOD relationships in terms

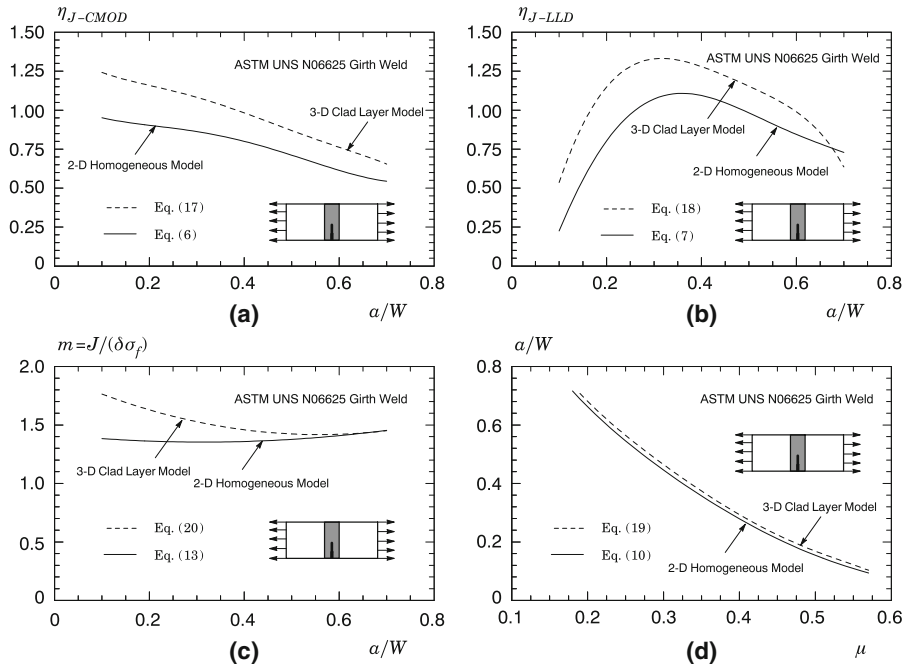


**Fig. 4** Comparison of plane-strain strain results for a homogeneous material with $n = 9.7$ (*solid lines*) and 3-D results for the tested weld centerline notched SE(T) specimens having a clad layer (*dashed lines*): **a** Geometric factor $\eta_{J-CMOD}$. **b** Geometric factor $\eta_{J-LLD}$. **c** $J-$CTOD relationship in terms of parameter $m$. **d** Elastic compliance relationship

of parameter $m$ for both the plane-strain and 3-D models are similar and (3) the 3-D elastic compliance for the weld centerline notched SE(T) specimen having a clad layer is similar to the plane-strain compliance.

The response displayed in Fig. 4 deserves further comments. Consider first the behavior of the $\eta$-factors shown in the plots of Fig. 4a, b, which can be understood in terms of the effect of the dissimilar material (undermatch weld metal and clad layer) on the plastic work and, consequently, on $J$. Recall Eq. (3) which can be manipulated to yield the $\eta$-factor as a function of $J_p/A_p$ so that changing the plastic work in terms of the plastic area under the $P-$CMOD curve due to the effect of the dissimilar material also affects the corresponding $\eta$-value [see also Kirk and Dodds (1992), and Paredes and Ruggieri (2012)]. Observe that this effect appears to play a lesser role on the $J-$CTOD relationship given in Fig. 4c as the variation of parameter $m$ with $a/W$ is relatively insensitive to the influence of dissimilar material in the present analysis, particularly for moderate to deep cracks ($a/W \gtrsim 0.3$). Consider now the dependence of normalized specimen compliance on $a/W$ shown in Fig. 4d. Because the variation of specimen compliance with crack length derives from an elastic analysis, the functional relationship between $a/W$ and normalized compliance, $\mu$, is little affected by whether plane-strain or full 3-D conditions are utilized in the numerical computations. Observe that the comparisons are made in terms of the normalized compliance not the absolute relationship between crack size and applied load. Indeed, these results exhibit trends similar to those given in recent work of Souza and Ruggieri who showed that the normalized compliance for common fracture specimens derived from 3-D analyses, including the normalized compliance values for the side-grooved models, are virtually indistinguishable from the compliance relationships derived from plane-strain analyses. Further observe that both plane-strain and 3-D analyses are performed on weld centerline notched specimens in which the weldment undermatches the base plate material so that the elastic properties of the weld metal (rather than the base plate material) are likely to dominate the (global) elastic response. This is exactly the result found in Fig. 4d in which the plane strain solution derived from elastic analyses for a homogeneous material with its elastic modulus assigned the value for the weld metal given in Table 1 is similar to the 3-D solution.

### 5.2 $J$-Resistance curves

The framework to determine $J$-resistance curves based on load–CMOD data described previously provides the basis for characterizing the ductile fracture response of

the tested CRA girth weld. All the results presented in this section consider the effects of crack growth on $J$ and, further, the influence of specimen rotation on specimen compliance with increased applied loading. In particular, Mathias et al. (2013) show that the measured fracture resistance curves derived from considering the effect of crack growth correction on $J$ are reduced by 10−15% when compared with the corresponding resistance data with no crack growth correction. While this effect appears to be less important in characterizing the crack growth response of the material for small amounts of ductile tearing, $\Delta a \lesssim 1-1.5$ mm, it may affect proper evaluation of the CTOD-resistance curve directly from $J$. This aspect will be taken up later in Sect. 5.4.

Figure 5 shows the measured crack growth resistance curves for the tested SE(T) specimens in which $J$ and $\Delta a$ are evaluated using plane-strain solutions for $\eta$ and $\mu$ applicable to a homogeneous material having flow properties corresponding to those for the weld metal. This is equivalent to assuming that the entire bulk of the specimen has the same flow properties as the weld metal—a condition usually referred to as all weld metal (AWM). As the figure indicates, the solid symbol corresponds to one of the specimens which was instrumented with a double clip gage fixture as required for CMOD measurements at two different points. The overall trend of increased $J$-values with increased amounts of ductile tearing is evident in this plot. Overall, the crack growth response derived from the present test procedure appears to be highly describable by the tested SE(T) specimens to serve as a basis for ductile tearing assessments in ECA procedures applicable to clad pipeline girth welds and similar structural components. Another evident feature in Fig. 5a is the "crack backup" (or apparent negative crack growth) observed in the initial part of the $J-R$ curves for both tested specimens. Despite the rotation correction adopted to evaluate the specimen compliance as briefly described previously, the early compliance measurements display an increase in specimen stiffness with increased loading for $0 \leq \Delta a \leq 0.5$ mm. However, such behavior appears to be a recurring feature with this specimen geometry as reported in early works of Joyce et al. (1993) and Joyce and Link (1995), and more recently by Drexler et al. (2010). While the precise causes of this phenomenon are not yet fully understood, it may be associated with non-straightness of the crack front after fatigue pre-cracking and large localized deformation at the clamp region early in the test thereby increasing the loading without any measurable increase in CMOD.

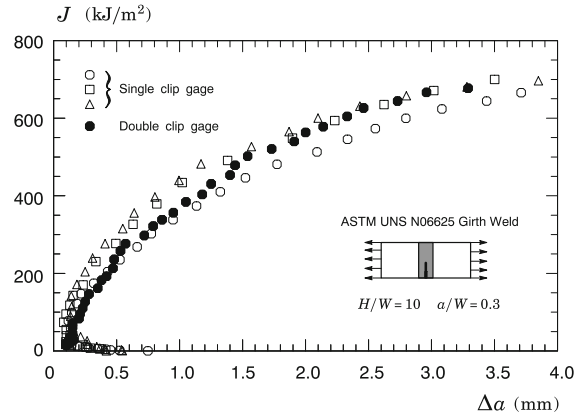


**Fig. 5** $J$-resistance curves including crack growth correction for the tested clamped SE(T) specimens based on plane-strain $\eta$-factors for a homogeneous material (AWM). The *solid symbol* corresponds to one of the specimens which was instrumented with a double clip gage fixture as required for CMOD measurements at two different points

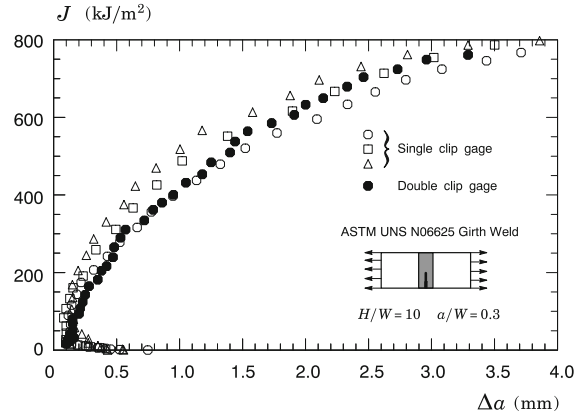


**Fig. 6** $J$-resistance curves including crack growth correction for the tested clamped SE(T) specimens based on 3-D $\eta$-factors including the effect of the undermatch weld and clad layer

Figure 6 displays the fracture resistance curves based on 3-D $\eta$-factors including the effect of the undermatched weld and clad layer developed in the previous section (refer to Fig. 4). The trend is clear. The $J$-resistance curves derived from more accurate $\eta$-factor solutions (recall that the elastic compliance solutions are essentially unaffected by the weld and clad layer) are ∼15% higher than the corresponding fracture resistance data obtained from plane-strain $\eta$-factors. This behavior can be understood by considering the undermatch condition of the weldment; here, for a given

**Table 2** Predicted and measured crack extension for all tested fracture specimens using a 9-point averaging procedure

| Specimen | Measured post test | | | Compliance estimation | | | |
|---|---|---|---|---|---|---|---|
| | $a_0$ (mm) | $a_f$ (mm) | $\Delta a$ (mm) | $a_0$ (mm) | $a_f$ (mm) | $\Delta a$ (mm) | Deviation (%) |
| CP4 | 5.0 | 10.6 | 5.6 | 5.0 | 9.7 | 4.7 | 16.3 |
| CP5 | 4.7 | 10.6 | 5.8 | 4.8 | 11.0 | 6.2 | 6.3 |
| CP6 | 4.8 | 9.6 | 4.8 | 5.0 | 8.9 | 3.8 | 19.7 |
| CP7 | 4.4 | 8.1 | 3.7 | 4.7 | 8.0 | 3.3 | 9.9 |

applied (remote) displacement at the specimen ends, the crack driving forces, such as $J$, should be higher when compared to the crack driving forces in the same specimen made of a homogeneous material. Perhaps more importantly, it becomes clear that this behavior (coupled with inclusion of crack growth correction) adds up to obtaining higher CTOD resistance curves when converted from $J-\Delta a$ data. This issue will be taken up again in Sect. 5.4.

### 5.3 Crack extension measurements

After the crack growth tests, all specimens were subjected to fatigue cycling (similar to the standard pre-crack fatigue cycling) before being broken apart to mark the new crack front and the amount of ductile tearing. A typical crack surface obtained from one of the SE(T) specimens is illustrated in Fig. 7a, which also includes the optical crack front profile displaying the crack length measured at nine or five equally spaced points centered about the specimen centerline - the use of a 5-point average procedure to measure crack extension will be addressed later. It can be seen that the specimen exhibited a somewhat non-uniform fatigue pre-crack most likely caused by microstructural heterogeneities at the crack front promoted by the welding process. Following standard methods based on the 9-point average technique, such as the procedure given by ASTM E1820 (American Society for Testing and Materials 2011b), the initial and final crack length measured by means of an optical method are compared with crack length estimates derived from the UC method. Figure 7b shows a typical fracture surface morphology to identify the primary fracture micromechanism operating during the ductile fracture process observed by a scanning electron microscope (SEM). Here, small inclusions are observed within a dimple structure thereby characterizing well a ductile fracture mode associated with substantial plastic deformation. Similar features are also observed for the crack surface of other test specimens.

Table 2 provides the predicted and measured crack extension for all tested fracture specimens in which the deviation between the predicted crack growth, $\Delta a_p$, and measured crack extension, $\Delta a_m$, is defined as $\Lambda = |\Delta a_p - \Delta a_m|/\Delta a_m$. These results reveal that crack extension prediction for two of the tested specimens (CP4 and CP6) derived from the UC procedure is not in good agreement with the measured amount of ductile tearing; here, the unloading compliance method underestimates the 9-point average crack extension by $15-20\%$ thereby plausibly producing an apparent higher $J$-resistance curve. In contrast, the predicted amount of crack extension for specimens CP5 and CP7 is in relatively good accord with the measured crack growth and shows a deviation of $5-10\%$ between the predicted and measured data. It is worth noting that several recent procedures to measure ductile tearing properties of pipeline girth welds using SE(T) specimens (Upstream ExxonMobil 2010; Ruggieri and Hippert 2015; Pussegoda et al. 2014) advocate a maximum deviation, $\Lambda_{max} = 15\%$, as a validity criterion. While we have not investigated further the cause of the larger deviation between the predicted and measured amount of crack growth for specimens CP4 and CP6, we argue that the relatively strong, irregular crack front profile could be a plausible reason for the relatively poor agreement between the measured and predicted amount of ductile tearing. Indeed, further examination of the fracture surface displayed in Fig. 7b reveals a highly non-uniform fatigue pre-crack profile, particularly near the specimen side-groove region, coupled with a relatively severe reverse tunneling of the final crack front. Clearly, inclusion of measurement points closer to the specimen free surface into the averaging procedure does affect the average value of the measured amount of crack extension.

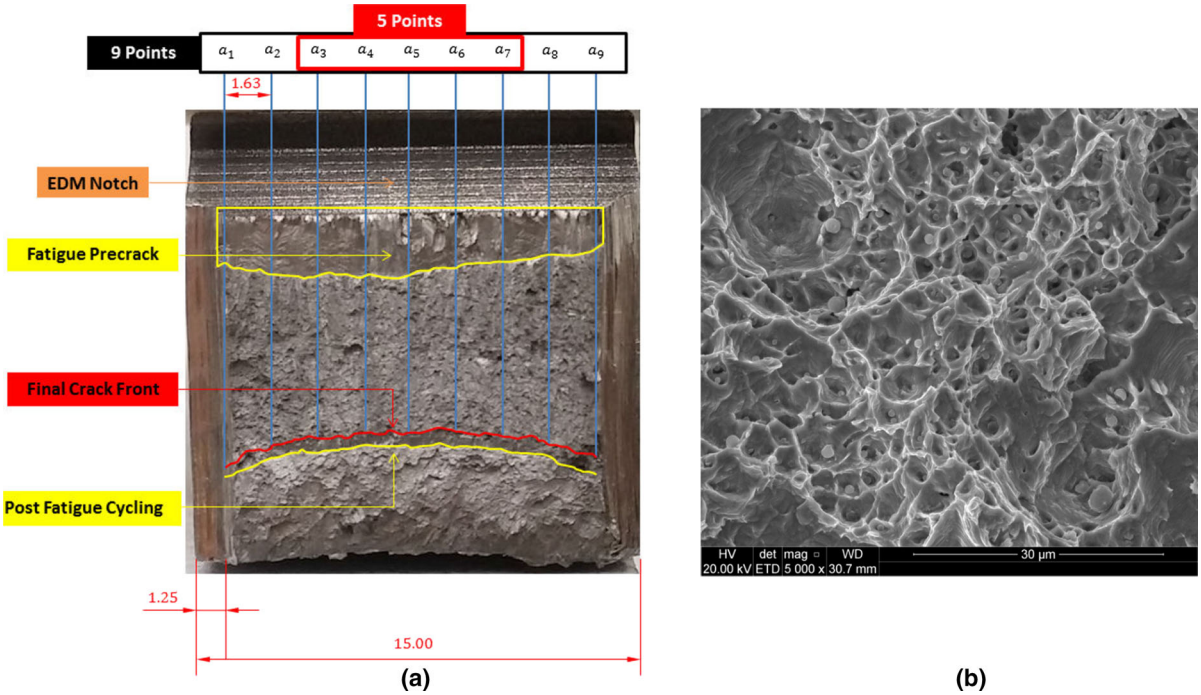


**Fig. 7** **a** Typical crack surface and the optical crack size measurement profile. **b** Typical fracture surface morphology observed by a scanning electron microscope (SEM) showing small inclusions within a dimple structure

**Table 3** Predicted and measured crack extension for all tested fracture specimens using a 5-point averaging procedure

| Specimen | Measured post test | | | Compliance estimation | | | |
|---|---|---|---|---|---|---|---|
| | $a_0$ (mm) | $a_f$ (mm) | $\Delta a$ (mm) | $a_0$ (mm) | $a_f$ (mm) | $\Delta a$ (mm) | Deviation (%) |
| CP4 | 5.1 | 10.3 | 5.2 | 5.0 | 9.7 | 4.7 | 10.4 |
| CP5 | 4.8 | 10.3 | 5.5 | 4.8 | 11.0 | 6.2 | 12.5 |
| CP6 | 4.9 | 9.2 | 4.3 | 5.0 | 8.9 | 3.8 | 10.5 |
| CP7 | 4.5 | 8.1 | 3.6 | 4.7 | 8.0 | 3.3 | 7.8 |

To illustrate this issue, Table 3 gives again the predicted and measured crack extension for the tested fracture specimens but with $\Delta a_m$ derived from a 5-point average procedure. Figure 7b shows the method in which the two outermost measurement points (at each specimen side) were removed from the averaging process. This approach can be justified by the following argument. In routine defect assessment procedures applicable to surface cracks, such as those typically found in pipeline girth welds with circumferential, semi-elliptical surface flaws, the primary interest usually lies in determining the crack driving forces at the deepest point of the semi-elliptical shaped crack. Consequently, the adoption of an averaging procedure which assigns more weight to crack growth measurements at the specimen center plane seems more consistent. Using this method, the results shown in the table now reveal a rather more uniform deviation in the range 8−13% which nevertheless satisfies the validity criterion of $\Lambda_{max} = 15\%$ as discussed before. Moreover, Fig. 8 compares the predicted and measured crack sizes (both the initial, $a_0$, and final, $a_f$, crack lengths are included in the plots) based on different averaging techniques. A reference line indicating $a_{0,m} = a_{0,p}$ and $a_{f,m} = a_{f,p}$ is provided on the figures to aid in assessing the relative deviation. The measured initial crack sizes are in remarkably close agreement with the corresponding predicted values for both averag-

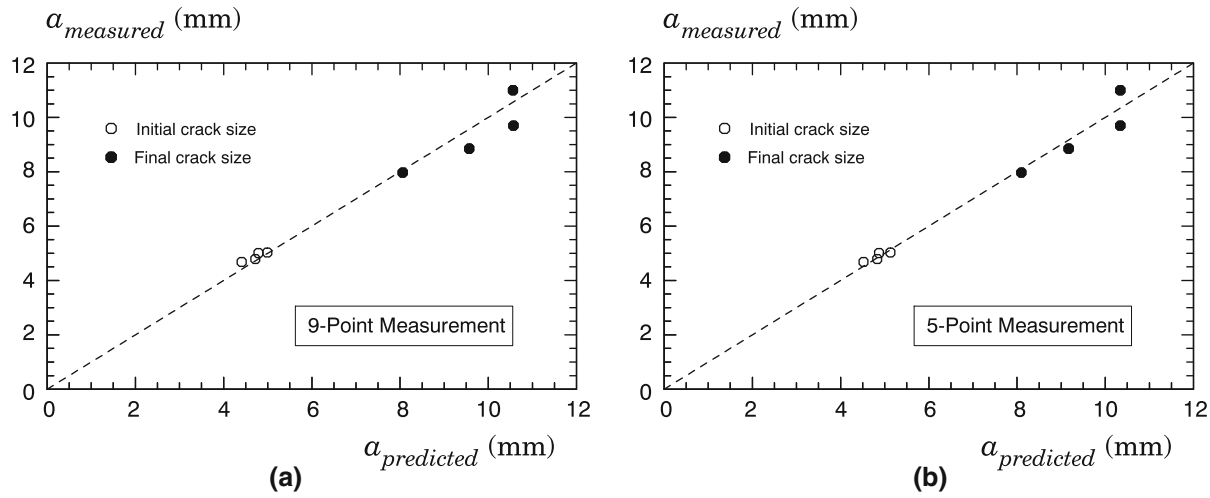


**Fig. 8** Comparison of predicted and measured crack sizes (initial and final crack lengths) based on different averaging procedures: **a** 9-point averaging method. **b** 5-point averaring method

ing methods. The predicted values for the final crack sizes display somewhat larger deviations compared to the corresponding measured values, particularly when the 9-point averaging method is utilized. Overall, however, these measurements compare well indicating the effectiveness of the unloading compliance procedure to evaluate crack growth resistance curves for the tested CRA girth weld.

### 5.4 CTOD resistance curves

Current defect assessment procedures applicable to piping components, including marine steel catenary risers (SCRs), often adopted by the oil and gas industry favor the use of CTOD$-R$ curves (rather than $J-\Delta a$ data) to define useful toughness values to characterize the material fracture resistance. These methodologies have evolved over the past few years to rely almost entirely on CTOD measurements derived from the double clip gage (DCG) technique outlined previously. While the merits and drawbacks of this approach remain debatable (see discussion in Sarzosa et al. (2015), it undoubtedly simplifies the procedure to evaluate the CTOD but at an extra cost of measuring two crack opening displacements. To facilitate interpretation of the ductile tearing response for the tested nickel–chromium CRA girth weld, we also provide crack growth resistance data in terms of CTOD$-\Delta a$ curves in which the crack tip opening displacement derives from the experimentally measured plastic area under the load versus crack mouth opening displacement (CMOD) curve and from direct measurements using the DCG technique. This study also explores further direct measurements of CTOD by comparing the fracture resistance curve obtained from using a digital image correlation (DIC) method with the corresponding CTOD$-R$ curve based on the DCG technique addressed in the next section.

Consider first the CTOD$-\Delta a$ curves for the tested girth weld shown in Fig. 9 in which the crack tip opening displacement is determined from the $J-$CTOD relationship defined by Eq. (11) with parameter $m$ evaluated by means of Eq. (20)—these $m$-values thus correspond to the 3-D analysis of the weld centerline notched SE(T) specimens having a clad layer. Because of the essentially linear relationship between $J$ and CTOD defined by Eq. (11), it is clear that Fig. 9 reproduces the same features already discussed before for the fracture resistance curves displayed in Fig. 5. For amounts of stable crack growth of $\approx$1mm, the CTOD-value is in the range of 0.40$-$0.45 mm.

Evaluation of fracture resistance in terms of CTOD based on the DCG method is considered next. Here, only the load–displacement data measured from testing the specimen equipped with a double-clip gage fixture is used to generate the CTOD$-R$ curve displayed in Fig. 10. To facilitate comparisons with the previous results, the CTOD resistance curves obtained by using the $J-$CTOD relationship shown in Fig. 9 are also included in the plot. The DCG-based resistance curve is consistently higher than the CTOD$-\Delta a$

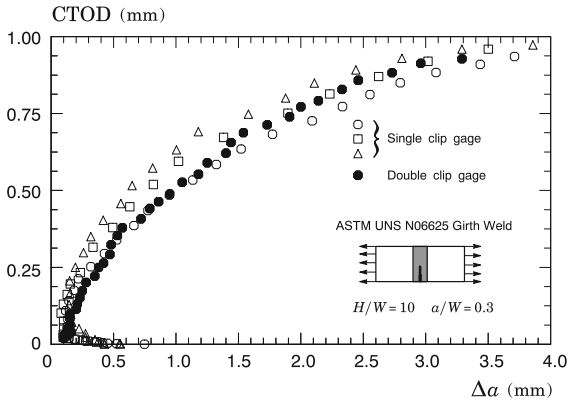


**Fig. 9** CTOD-resistance curves including crack growth correction for the tested clamped SE(T) specimens derived from the $J-$CTOD relationship defined by Eq. (11) in which parameter $m$ is evaluated by means of Eq. (20)

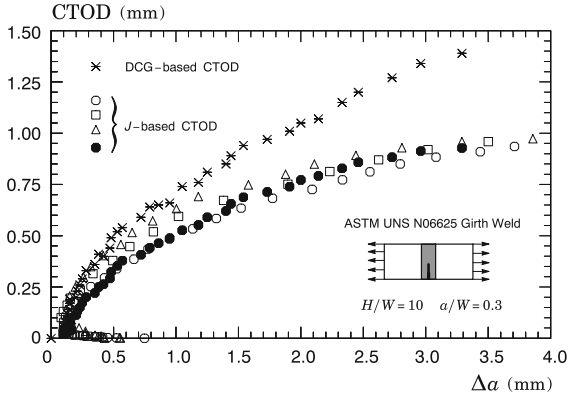


**Fig. 10** CTOD-resistance curve derived from the double clip-gage (DCG) method for the tested SE(T) specimen instrumented with a double clip gage fixture

data based on $J$, particularly for larger amounts of stable crack growth, say $\Delta a \gtrsim 1.5$ mm. Here, differences between both methods range from $\sim$25% for $\Delta a = 1.5$ mm to $\sim$45% for $\Delta a = 3$ mm. Observe, however, that the CTOD resistance data based on DCG measurements increase steadily with crack growth for $\Delta a > 1.0$ mm such that the corresponding tearing modulus, which can be simply defined as $d\delta/da$ (Anderson 2005), remains essentially constant. In contrast, the $J$-based CTOD resistance curves also increase with increased $\Delta a$ but at a much lower rate as characterized by much smaller values of $d\delta/da$ , particularly at larger amounts of ductile tearing. Allowing for some uncertainties and difficulties associated with double clip-gage measurements, these results seem generally consistent with our previous contention that, because our developed $J-$CTOD relationship includes effects of crack growth on $J$, the associated CTOD resistance curve should be lower than the DCG-based resistance curve. Moreover, at large deformation levels (which correspond to larger amounts of stable crack growth), much of the total work done by the applied (remote) loading is likely dissipated into background plasticity thereby reducing the plastic contribution to the strain energy for the cracked body in terms of $J$. In contrast, because the CTOD based on DCG derives from a rather simple measurement of the relative displacements of the crack profile [refer again to Fig. (1)], it keeps increasing with increased loading. Thus, it becomes clear that the DCG-based resistance curve results in non-conservative toughness values at fixed amounts of stable crack growth thereby potentially impacting adversely ECA assessments. Currently, we consider these differences in CTOD measurements an open issue. An investigation along this line of investigation is in progress and will be presented in a forthcoming publication.

### 5.5 Digital image correlation measurements of CTOD

Concurrent with measurements of the CTOD for the growing crack based on the double clip-gage technique described in Sect. 2.3, an improved optical measurement method was also utilized to measure the CTOD with increased amounts of ductile tearing for the tested specimens. Using a digital image correlation (DIC) method to determine the relative displacement fields for different digital images of the cracked specimen with increased deformation, the deformed crack flank and, thus, the CTOD can be evaluated in straightforward manner. By recording a series of images during the test, each one divided into a grid of subsets, the DIC displacement measurements follow from correlating the displacement fields for the subsets at different deformation states thereby estimating the displacement field from one image to the following one. In the present study, an 8-megapixel, monochromatic digital camera was used for image acquisition. Correlated Solutions VIC-2D V6.0 software was used for all data acquisition, calibration and DIC data analysis. Readers are referred to Sutton et al. (2009) and references therein for full details on the DIC method.

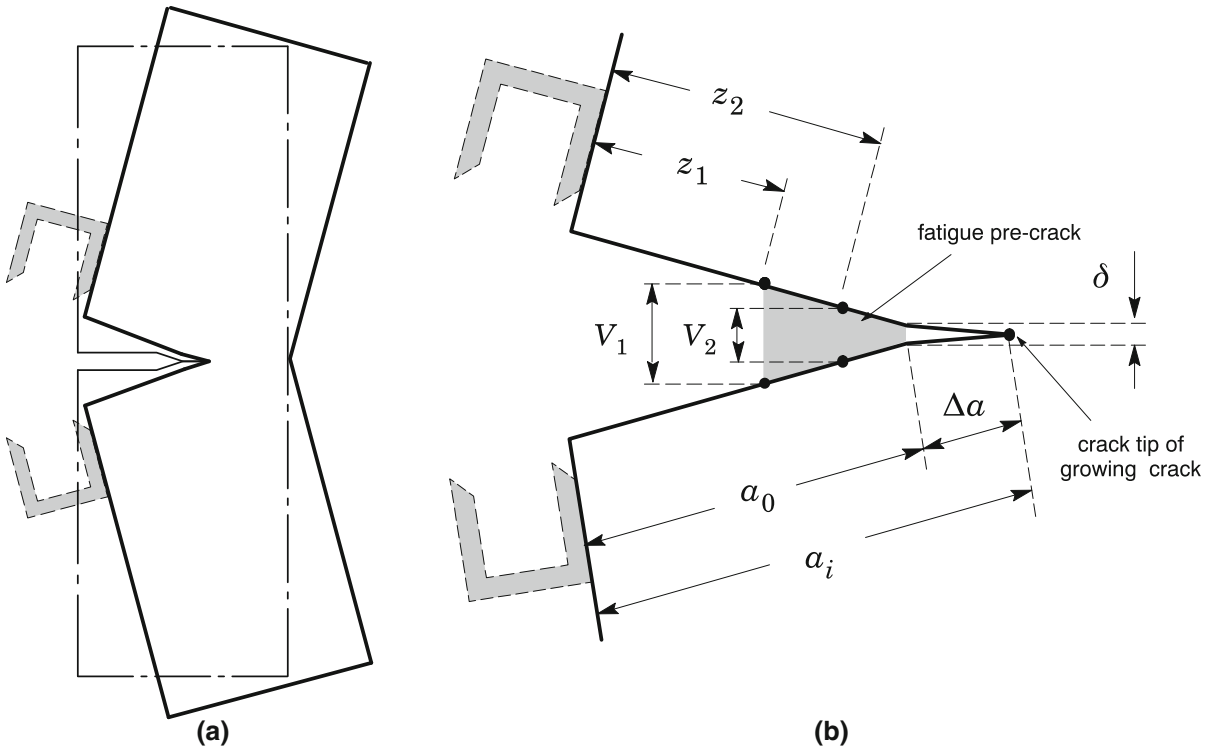


**Fig. 11** DIC measurement scheme based on placing the measurement points on the fatigue pre-crack flank slightly behind the extending crack flank

CTOD-values during crack growth in the SE(T) specimen are evaluated from DIC measurements using the scheme displayed in Fig. 11, which is based on placing the measurement points on the fatigue pre-crack flank slightly behind the extending crack flank. As already outlined in previous Sect. 2.3, since the DCG mounting fixture is typically installed at a distance $x_0$ from the notch flank indicated in Fig. 1b, placing the measurement points on the deformed flanks of the fatigue pre-crack presumably provides a better characterization of the local displacement fields than the DCG method (which may result in an apparent increase of the measured CTOD value as also indicated in Fig. 1). Consequently, we can anticipate a more accurate evaluation of the CTOD for the growing crack even though the CTOD ($\delta$) is still defined at the original crack tip position—see Fig. 11b in which the CTOD is defined as the crack opening at the crack length $a_0$. Here, by measuring two COD-values, $V_1$ and $V_2$, at two locations on the fatigue pre-crack flank, the CTOD is determined in straightforward manner by simple triangulation.

Figure 12 displays the CTOD resistance curve based on DIC measurements of crack opening displacements for the fatigue pre-crack flank. To facilitate comparisons, the DIC measurements are performed on the same tested SE(T) specimen instrumented with a double clip gage fixture. The previous results for the CTOD$-R$ curves are also included to aid in assessing the relative change in fracture resistance data. This figure shows clearly the effect of different measurement points (upon which the triangulation defining parameter $\delta$ is based) on the CTOD-value. The DIC-based CTOD resistance curve is now closer to the fracture resistance curves obtained by using the $J-$CTOD relationship. In particular, the DIC-based data agrees well with the CTOD$-R$ curves derived from $J$ for amounts of ductile tearing in the range $\Delta a \leq 2$ mm. Observe, however, that the CTOD resistance data based on DIC measurements also increase steadily with crack growth for $\Delta a > 2$ mm such that the corresponding tearing modulus remains essentially constant—this behavior is similar to the DCG-based CTOD$-R$ curve shown in previous section.

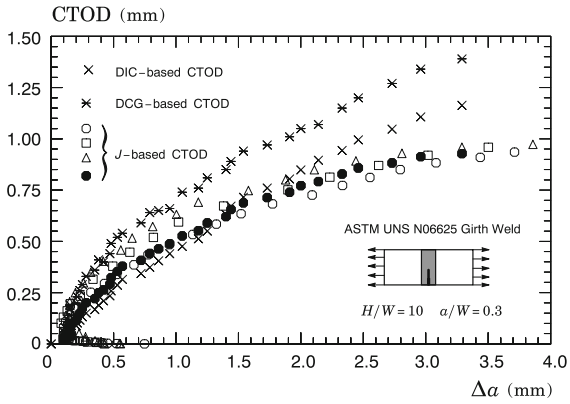


**Fig. 12** CTOD-resistance curve derived from measurements of crack opening displacements for the fatigue pre-crack flank using a digital image correlation (DIC) technique

## 6 Summary and conclusions

This study presents an exploratory experimental investigation of the crack growth resistance properties for the girth weld of an API 5L Grade X65 internally clad with a nickel–chromium corrosion resistant alloy (CRA) of ASTM UNS N06625 Alloy 625. Testing of the pipeline girth welds employed side-grooved, clamped SE(T) specimens with a weld centerline notch to determine the crack growth resistance curves based upon the unloading compliance (UC) method using a single specimen technique. The experiments and fracture resistance data described in this paper show the effectiveness of the UC procedure to characterize ductile tearing properties for dissimilar girth weld materials which serve as a basis for ductile tearing assessments in ECA procedures applicable to clad pipeline girth welds and similar structural components.

A central observation emerging from our work is the rather strong dependence of the CTOD$-R$ curves on the evaluation method of the crack tip opening displacement for the extending crack. In previous study of Sarzosa et al. (2015), it has been found that the CTOD-values derived from the double clip-gage (DCG) method agree well with the corresponding CTOD-values computed for the growing crack based on $J-$CTOD relationships. However, we should point out that those comparisons for both definitions of CTOD derive from finite element analyses in which two COD-values at two locations on a straight line passing through the crack flank of the numerical model are continuously computed with increased load levels as characterized by $J$. In the fracture tests, the DCG-based CTOD appears to be sensitive to a certain degree to the (correct) setup of the double clip gage fixture which equips the SE(T) specimen. Perhaps more importantly, though, our results show rather convincingly that the CTOD evaluation procedure based on the DCG technique shows a clear tendency to provide higher fracture resistance curves and, consequently, non-conservative fracture assessments. In contrast, DIC measurements of CTOD based on crack flank measurement points provide good agreement with the CTOD$-R$ curve evaluation procedure based on the developed $J-$CTOD relationship for the clad SE(T) specimen. The analyses and test results described here thus suggest that the use of CTOD$-R$ curves to measure crack growth properties for pipeline girth welds and similar structural components based on $J-$CTOD relationships may eliminate the potential non-conservatism that would otherwise arise when using DCG-based CTOD$-R$ curves. Clearly, more experimental and analytical studies are needed to clarify the significance of CTOD measurements for growing cracks—this issue appears central to develop a more robust and meaningful CTOD-resistance evaluation procedure. Additional work is in progress along this line of investigation covering crack growth resistance testing based on the UC procedure of two widely different hardening steels using clamped SE(T) fracture specimens.

**Acknowledgements** This investigation is supported by the Brazilian Council for Scientific and Technological Development (CNPq) through Grants 473975/2012-2 and 306193/2013-2. The second author (VSB) is supported by the CAPES Foundation and Brazilian Ministry of Education through a Ph.D. scholarship. The authors acknowledge Petrobras for providing additional support for the work described here and for making available the experimental data. The authors are also indebted to Professor Celso Pupo Pesce (University of São Paulo) for his assistance in implementing the digital image correlation (DIC) system. Helpful discussions with Dr. Rafael G. Savioli (University of São Paulo) are also acknowledged.

## References

American Petroleum Institute (2007a) Fitness-for-service, API RP-579-1/ASME FFS-1

American Petroleum Institute (2007b) Specification for line pipe, API 5L

American Society for Testing and Materials (2009) Standard specification for nickel–chromium-molybdenum–columbium alloy (UNS N06625) and nickel–chromium–

mlybdenum–silicon alloy (UNS N06219) plate, sheet, and strip, ASTM B443-00
American Society for Testing and Materials (2011a) Standard specification for nickel–chromium-molybdenum–columbium alloys (UNS N06625 and UNS N06852) and nickel–chromium–molybdenum–silicon alloy (UNS N06219) pipe and tube, ASTM B444-06
American Society for Testing and Materials (2011b) Standard test method for measurement of fracture toughness, ASTM E1820-2011
American Society for Testing and Materials (2011c) Standard test methods for tension testing of metallic materials, ASTM E8-11
American Society for Testing and Materials (2015) Standard test method for measurement of fracture toughness, ASTM E1820-2015
Anderson TL (2005) Fracture mechanics: fundaments and applications, 3rd edn. CRC Press, Boca Raton
British Institution (2014) Method of test for determination of fracture toughness in metallic materials using single edge notched tension (SENT) specimens, BS 8571
Cravero S, Ruggieri C (2005) Correlation of fracture behavior in high pressure pipelines with axial flaws using constraint designed test specimens–part I: plane-strain analyses. Eng Fract Mech 72:1344–1360
Cravero S, Ruggieri C (2007a) Estimation procedure of J-resistance curves for SE(T) fracture specimens using unloading compliance. Eng Fract Mech 74:2735–2757
Cravero S, Ruggieri C (2007b) Further developments in J evaluation procedure for growing cracks based on LLD and CMOD data. Int J Fract 148:387–400
Det Norske Veritas (2013) Submarine pipeline systems, Offshore Standard OS-F101
Drexler E, Wang Y-Y, Sowards JW, Dvorak MD (2010) SE(T) testing of pipeline welds. In: 8th international pipeline conference (IPC), Calgary, Canada
Healy B, Gullerud A, Koppenhoefer K, Roy A, RoyChowdhury S, Petti J, Walters M, Bichon B, Cochran K, Carlyle A, Sobotka J, Messner M, Dodds RH (2014) WARP3D: 3-D nonlinear finite element analysis of solids for fracture and fatigue processes, technical report, University of Illinois at Urbana–Champaign. http://code.google.com/p/warp3d
Huang Y, Zhou W (2014) J-CTOD relationship for clamped SE(T) specimens based on three-dimensional finite element analyses. Eng Fract Mech 131:643–655
Hutchinson JW (1983) Fundamentals of the phenomenological theory of nonlinear fracture mechanics. J Appl Mech 50:1042–1051
Joyce JA, Hackett EM, Roe C (1993) Effects of crack depth and mode loading on the J–R curve behavior of a high strength steel. In: Underwood JH, Schwalbe K-H, Dodds RH (eds) Constraint effects in fracture, ASTM STP 1171. American Society for Testing and Materials, Philadelphia, pp 239–263
Joyce JA, Link RE (1995) Effects of constraint on upper shelf fracture toughness. In: Reuter WG, Underwood JH, Newman J (eds) Fracture mechanics, ASTM STP 1256. American Society for Testing and Materials, Philadelphia, pp 142–177
Kanninen MF, Popelar CH (1985) Advanced fracture mechanics. Oxford University Press, New York
Kirk MT, Dodds RH (1992) Effect of weld strength mismatch on elastic–plastic fracture parameters, structural research series (SRS 570) UILU-ENG-92-2008. University of Illinois at Urbana–Champaign
Kirk MT, Dodds RH (1993) J and CTOD estimation equations for shallow cracks in single edge notch bend specimens. J Test Eval 21:228–238
Kirk MT, Wang Y-Y (1995) Wide range CTOD estimation formulae for SE(B) specimens. In: Reuter WG, Underwood JH, Newman J (eds) Fracture mechanics, ASTM STP 1256. American Society for Testing and Materials, Philadelphia, pp 126–141
Kudari SK, Kodancha KG (2008) On the relationship between *J*-integral and CTOD for CT and SENB specimens. Frattura ed Integrità Struttturale 6:3–10
Mathias LLS, Sarzosa DFB, Ruggieri C (2013) Effects of specimen geometry and loading mode on crack growth resistance curves of a high-strength pipeline girth weld. Int J Press Vessels Pip 111–112:106–119
Nyhus B, Polanco M, Ørjasæter O, (2003) SENT specimens as an alternative to SENB specimens for fracture mechanics testing of pipelines. In: 22nd international conference on ocean, offshore and arctic engineering (OMAE), Vancouver, Canada
Paredes M, Ruggieri C (2012) Further results in J and CTOD estimation procedures for SE(T) fracture specimens—part II: weld centerline cracks. Eng Fract Mech 89:24–39
Pussegoda N, Tiku S, Tyson W (2014) Measurements of crack-tip opening displacement (CTOD) and *J*-fracture resistance curves using single-edge notched tension (SENT) specimens, technical report 30166-001-R01, BMT Fleet Technology
Ruggieri C (2012) Further results in J and CTOD estimation procedures for SE(T) fracture specimens—part I: homogeneous materials. Eng Fract Mech 79:245–265
Ruggieri C, Hippert E (2015) Test procedure for fracture resistance characterization of pipeline steels and pipeline girth welds using single-edge notched tension (SENT) specimens. University of São Paulo, technical report
Sarzosa DFB, Ruggieri C (2014) Relationship between *J* and CTOD in SE(T) and SE(B) specimens for stationary and growing cracks. In: 10th international pipeline conference (IPC 2014), Calgary, Canada
Sarzosa DFB, Souza RF, Ruggieri C (2015) *J*-CTOD relations in clamped SE(T) fracture specimens including 3-D stationary and growth analysis. Eng Fract Mech 147:331–354
Shen G, Tyson WR (2009) Crack size evaluation using unloading compliance in single-specimen single-edge notched tension fracture toughness testing. J Test Eval 37(4):347–357
Shen G, Bouchard R, Gianetto JA, Tyson WR (2008) Fracture toughness evaluation of high-strength steel pipe. In: ASME PVP 2008 pressure vessel and piping division conference, American Society of Mechanical Engineers, Chicago, IL
Shih CF (1981) Relationship between the J-integral and the crack opening displacement for stationary and extending cracks. J Mech Phys Solids 29:305–326
Silva LAL, Cravero S, Ruggieri C (2006) Correlation of fracture behavior in high pressure pipelines with axial flaws using constraint designed test specimens—part II: 3-D effects on constraint. Eng Fract Mech 76:2123–2138

Souza RF, Ruggieri C (2016) Revised wide range compliance solutions for selected standard and non-standard fracture test specimens based on crack mouth opening displacement. Eng Fract Mech **(Submitted for Publication)**

Sutton MA, Orteu JJ, Schreier H (2009) Image correlation for shape, motion and deformation measurements. Springer, Berlin

Upstream ExxonMobil (2010) Measurements of crack-tip opening displacement. (CTOD) fracture resistance curves using single-edge notched tension (SENT) specimens, technical report

Zhu XK, Joyce JA (2012) Review of fracture toughness (G, K, J, CTOD, CTOA) testing and standardization. Eng Fract Mech 86:1–46

Zhu XK, McGaughy T (2014) A review of fracture toughness testing and evaluation using sent specimens. In: 10th international pipeline conference (IPC), Calgary, Canada

Zhu XK, Leis BN, Joyce JA (2008) Experimental estimation of J–R curves from load-CMOD record for SE(B) specimens. J ASTM Int 5(5):1–15